PHYSICAL REVIEW B **79**, 045318 (2009)

SiC/Ti_3SiC_2 interface: Atomic structure, energetics, and bonding

Zhongchang Wang,[1,*] Susumu Tsukimoto,[1] Mitsuhiro Saito,[1] and Yuichi Ikuhara[1,2,†]

[1]*WPI Research Center, Advanced Institute for Materials Research, Tohoku University, 2-1-1 Katahira, Aoba-ku, Sendai 980-8577, Japan*

[2]*Institute of Engineering Innovation, The University of Tokyo, 2-11-16, Yayoi, Bunkyo-ku, Tokyo 113-8656, Japan*

(Received 26 November 2008; published 29 January 2009)

The structural, electronic, and adhesive properties of the 4H-SiC(0001)/Ti_3SiC_2(0001) interface are systematically investigated by first-principles calculations. A total of 96 candidate interface geometries are considered, encompassing four SiC terminations, each of which involves six Ti_3SiC_2 terminations and four stacking sequences. We find that the fundamental influence of the SiC substrate on the optimal Si-terminated interface is twofold characterized atomically by pulling the interfacial C atoms of Ti_3SiC_2 toward the positions that would normally be filled by C in bulk SiC and electronically by forcing the density of states projected on the interfacial C of Ti_3SiC_2 to approach that of C in bulk SiC rather than bulk Ti_3SiC_2. Consequently, the interfacial C of Ti_3SiC_2 is reasonably viewed as a natural extension of the C sublattice of bulk SiC across the interface. In contrast, atomic relaxation in the optimal C-terminated interface results in minor rearrangement, wherein the interfacial C of Ti_3SiC_2 rests straight above interfacial C of SiC. Regardless of the relaxation and SiC terminations, adhesion is found to be sensitive to choice of Ti_3SiC_2 termination and interfacial C to be an important factor influencing adhesion strength. Using several analytic techniques, we have characterized the electronic structures thoroughly and determined the interfacial bonding to be of a mixed covalent-ionic nature.

DOI: 10.1103/PhysRevB.79.045318 PACS number(s): 68.35.−p

I. INTRODUCTION

The promising mechanical and electronic properties of silicon carbide (SiC) are stimulating extensive investigations focused on exploiting its semiconducting and excellent structural properties. In fact, the interest toward SiC is twofold. On one hand, it is a high-strength composite and high-temperature structural ceramic,[1] demonstrating the ability to function in extremely high friction and radiation conditions.[2,3] On the other hand, it is an attractive semiconductor[4,5] with excellent inherent characteristics such as a wide band gap, high breakdown field, and more than double the high carrier mobility and electron saturation drift velocity of silicon.[6,7] These intrinsic electronic properties make it the most likely of all wide band-gap semiconductors to succeed Si in next-generation electronic devices, especially for high power and frequency applications.[8,9] Successful fabrication of SiC-based semiconducting devices include Schottky barrier diodes,[10] p-i-n diodes,[11,12] metal-oxide-semiconductor field effect transistors,[13] insulated gate bipolar transistors,[14] and so forth.

The wide use of SiC as an electronic component is currently limited by the absence of robust and low-resistance Ohmic contacts, which allow higher current driving, faster switching speed, and less power dissipation. Most of the studies that have been carried out to date to obtain Ohmic contacts to 4H-SiC (Refs. 15 and 16) have involved the deposition of Al alloys with Ti (Refs. 17 and 18) or Ni.[19,20] These deposited alloys are the only currently available materials that yield significantly low specific contact resistivity (Ohmic contact) to 4H-SiC. Moreover, they exhibit high thermal stability. The formation of Ohmic contacts has been reported to occur through the generation of silicide on the SiC substrate after annealing, serving as a primary current pathway to lower the Schottky barrier between the metal and semiconductor.[18,21] Several groups have later identified the unknown silicide as ternary Ti_3SiC_2 through x-ray diffraction analysis.[22,23] However, the role of the SiC/Ti_3SiC_2 interface on the mechanism whereby the Schottky barrier becomes Ohmic remains unclear. It is not even clear how the two materials atomically bond together because of experimental complications associated with the study of a buried interface. As in the case of other semiconducting materials,[24,25] detailed knowledge on the atomic and electronic structure of the SiC/Ti_3SiC_2 interface is essential to elucidate the mechanism and for device design and performance control.

To determine the most stable interface theoretically, one first has to establish feasible models on the basis of distinct terminations and contact sites and then compare them. However, a direct comparison of the total energies of such models is not physically meaningful since interfaces might have a different number of atoms. On the other hand the *adhesion energy* $\mathbf{W}_{ad}$,[26,27] which is the key to predicting the mechanical properties of the interface, is physically comparable. Generally, the $\mathbf{W}_{ad}$, which is defined as the reversible energy required to separate an interface into two free surfaces, can be expressed by the difference in total energy between the interface and isolated slabs,[28,29]

$$\mathbf{W}_{ad} \equiv (E_1 + E_2 - E_{IF})/A. \tag{1}$$

Here E_1, E_2, and E_{IF} are the total energies of isolated slab 1, slab 2, and their interface, respectively, and A is the total interface area. To date, analytic models for predicting $\mathbf{W}_{ad}$ concerning SiC have mostly been restricted to SiC/metal heterojunctions such as SiC/Ni,[30] SiC/Al,[31,32] and SiC/Ti.[33] These models are motivated by the experimental deposition of metals on SiC. However, they neglect the complexity of the situation; namely, the compounds can be generated on SiC after annealing and thus are only applicable to systems with an as-deposited state. To our knowledge, no theoretical study on the adhesion between SiC and the formed com-

 ©2009 The American Physical Society

pounds at the atomic scale has been performed despite the essential effect of this interface on TiAl-based contact systems.

Experimentally, transmission electron microscopy (TEM) studies by Tsukimoto *et al.*[22,34] provided rather detailed information on microstructure of the 4H-SiC/TiAl interface. They have found that 4H-SiC is covered entirely by Ti_3SiC_2 with the orientation relationships $(0001)_{Ti_3SiC_2} \| (0001)_{SiC}$ and $[0\bar{1}10]_{Ti_3SiC_2} \| [0\bar{1}10]_{SiC}$. The universal cover ensures exclusive contact of Ti_3SiC_2 to the 4H-SiC in the TiAl-based contact system. Further, high-resolution TEM (HRTEM) revealed that the 4H-SiC/Ti_3SiC_2 interfaces are atomically flat without contaminant, while some planar terraces and ledges were observed. Moreover, Gao *et al.*[35] confirmed—by characterizing composition and local states around the interface—that no additional Al segregates to the interface, which corroborates the clean contact of Ti_3SiC_2 to SiC. In light of these observations, we ignored the influence of any other possible contaminants that might not be detected and instead focused on clean interfaces and surfaces.

Although the interfacial orientation has been observed, it remains difficult to gain additional information from experiments. In particular, the atomic configuration and chemical environment at the interface, which strongly affect the physical properties, are hardly accessible. However, atomistic computations can offer a way of complementing experimental results. Furthermore, simulations, especially first-principles calculations, can yield insight into the bonding nature and contact preference of the heterostructure. Thus, in addition to determining the adhesion energies, we aim to systematically investigate the atomic and electronic structures of the 4H-SiC/Ti_3SiC_2 interface from first-principles calculations. 4H-SiC will hereafter be referred to as SiC. First, to identify the most stable structure, we considered a total of 96 candidate interface geometries to cover all possible terminations. Although Si-terminated SiC was employed in the experiment,[22] we have chosen to also present results for C-terminated SiC in order to draw a comparison with Si-terminated SiC and as a precursor to follow up the study of this interface. The second purpose of this work is to elucidate the nature of the interfacial bonds and thus shed light on the correlation of adhesion to electronic structure.

The remainder of this paper is organized as follows. Section II describes the computational methodology used and Sec. III presents detailed results on bulk and surface calculations. Section IV outlines the geometries of the 96 candidate interfaces and describes the procedure used to obtain their adhesion energies. The 96 interfaces are divided into two groups based on their SiC terminations: Si- and C-terminated interfaces. The results of adhesion energies, atomic structures, electronic states, and bonding characters for the Si-terminated interfaces are presented in Sec. V and those for C-terminated interfaces in Sec. VI. We provide concluding remarks in Sec. VII.

II. METHODOLOGY

Calculations of electronic structure and total energy were carried out using the Vienna *ab initio* simulation package (VASP) within the framework of density-functional theory (DFT).[36,37] The projector-augmented wave method[38] was used for electron-ion interactions and the generalized gradient approximation of Perdew *et al.*[39] (PW91) was employed to describe the exchange-correlation functional. The single-particle Kohn-Sham wave function was expanded using plane waves with different cut-off energies depending on the calculated systems. Sampling of irreducible Brillouin zone was performed with a regular Monkhorst-Pack grid of special k points[40] and electronic occupancies were determined according to the Methfessel-Paxton scheme.[41] Independent k point convergence tests were conducted for distinct supercells, ranging from the primitive cell of bulk up to the largest 120-atom cell. Ground-state charge densities were calculated self-consistently using a Pulay-type[42] mixing scheme and the stable blocked Davidson minimization algorithm.[43] Total energies were calculated using the linear tetrahedron method with Blöchl corrections,[44,45] which eliminates broadening-related uncertainties. All atoms were fully relaxed using the conjugate gradient algorithm[46] until the magnitude of the Hellmann-Feynman force[47] on each atom converged to less than 0.05 eV/Å, yielding optimized structures.

III. BULK AND SURFACE CALCULATIONS

A. Bulk properties

We first assess accuracy of the computational methods by performing bulk calculations. It is known that 4H-SiC, one of the most common SiC polymorphs,[48,49] belongs to the hexagonal $P6_3mc$ space group with $a=3.081$ Å and $c=10.085$ Å.[50,51] Ti_3SiC_2 also has a hexagonal structure but within the $P6_3mmc$ space group ($a=3.068$ Å and $c=17.669$ Å).[52,53] The Ti atoms of Ti_3SiC_2 occupy two types of nonequivalent positions: one (Ti1, two per unit cell) has C atoms as nearest neighbors, while the other (Ti2, four per unit cell) has Si atoms [Fig. 4(a)]. Bulk properties were calculated using a cut-off energy of 450 eV and $6\times6\times2$ k points, which converges total energies to less than 1 meV/atom. The calculated optimum lattice constants of bulk SiC are $a=3.095$ Å and $c=10.131$ Å, 100.5% of the experimental values;[51] while those of bulk Ti_3SiC_2 are $a=3.076$ Å and $c=17.713$ Å, 100.25% of the experimental values.[53] In addition, our calculated values are in excellent agreement with other reported results.[51,54]

The calculated energy band gap of SiC is 2.25 eV, which is smaller than the experimental value of 3.26 eV (Ref. 55) and the value of 3.30 eV calculated using self-interaction corrections pseudopotentials, as reported by Baumeier *et al.*[56] However, it is close to the calculated value of 2.18 eV reported by Käckell *et al.*[57] and the 2.43 eV reported by Ching *et al.*[58] Deviation from the experimental value is attributed to the well-known drawback of the DFT.[59,60] Overall features of band structure [Fig. 1(a)], however, agree well with previous calculations[57,58] and the location of calculated conduction-band (CB) minima is consistent with experimental data.[61,62] The valence band (VB) originates mainly from the bonding between the s and p states of Si and C in the form of sp^3 hybridization, as shown in Fig. 2(a). In contrast, Ti_3SiC_2 exhibits a metallic nature with bands crossing E_F

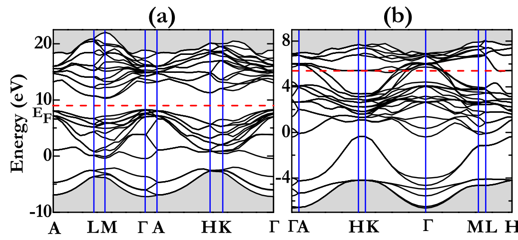

FIG. 1. (Color online) Energy-band structure of (a) 4H-SiC and (b) Ti_3SiC_2 along major symmetric directions. The horizontal and dashed lines denote the Fermi level (E_F).

[Fig. 1(b)] and thus resulting in a peak in total density of states (DOS) at E_F [Fig. 2(b)]. It is worth noting that the presence of the bands at E_F is caused by the energetic overlap of Ti d states with the gap levels of SiC [Fig. 2(b)], not an artifact due to the DFT underestimation of band gap. This metallic character is in agreement with reported experimental results[63] and other theoretical studies.[64,65] It is also clear from Fig. 2(b) that the contribution to the CB comes predominantly from antibonding Ti d states and that the VB is dominated by hybridized bonding states containing mainly p orbitals of Si and C and d orbitals of Ti.

B. Surface properties

Since the main goal of this study is to investigate the structure, adhesion, and bonding of the experimentally stimulated *bulklike* interface, it is essential to ensure that the two sides of the interface slabs used in calculations are thick enough to exhibit bulklike interiors because properties of a thin film may differ significantly from those of the bulk. To determine the minimum layer necessary for a bulklike slab, we first performed calculations on the convergence of surface energy with respect to slab thickness and then considered an additional series of surface relaxations as a function of slab layers. The surface energies of SiC (σ_S^0) and Ti_3SiC_2 (σ_T^0) under the condition that the chemical potential of the respective element equals its bulk total energy can be expressed as follows:

$$\sigma_S^0 = \frac{1}{2A}[E_{\rm slab}^{\rm total} - N_{\rm C}E_{\rm SiC}^{\rm bulk} - E_{\rm Si}^{\rm bulk}(N_{\rm Si} - N_{\rm C})], \qquad (2)$$

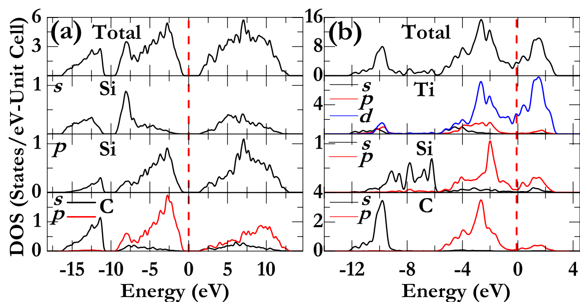

FIG. 2. (Color online) Total and partial densities of states (PDOSs) for (a) 4H-SiC and (b) Ti_3SiC_2. The PDOS of Ti includes those of Ti1 and Ti2. The Fermi level is set to zero.

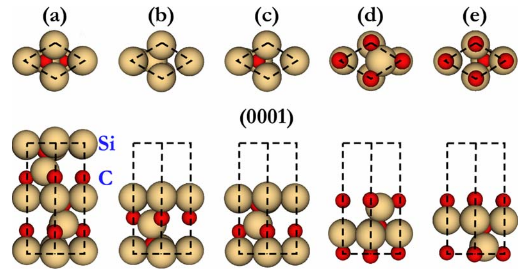

FIG. 3. (Color online) Schematic plot of 4H-SiC: (a) bulk, (b) Si1, (c) Si2, (d) C1, and (e) C2 terminations. The upper part shows the top view, while the lower one shows the side view. Only the top five of nine symmetric layers are presented for each termination.

$$\sigma_T^0 = \frac{1}{2A}\left[E_{\rm slab}^{\rm total} - \frac{1}{2}N_{\rm C}E_{\rm Ti_3SiC_2}^{\rm bulk} - E_{\rm Ti}^{\rm bulk}\left(N_{\rm Ti} - \frac{3}{2}N_{\rm C}\right) - E_{\rm Si}^{\rm bulk}\left(N_{\rm Si} - \frac{1}{2}N_{\rm C}\right)\right], \qquad (3)$$

where $E_{\rm slab}^{\rm total}$ and $E_X^{\rm bulk}$ denote total energies of a slab and X bulk, and N_Y and A represent the number of Y (Y=Ti, Si, C) atoms and surface area, respectively.

1. 4H-SiC(0001)

Experimentally, the SiC(0001) plane was observed to be a favorable substrate that allows epitaxial growth of Ti_3SiC_2 with also a (0001)-oriented face.[22,34] Four types of SiC termination within the (0001) surface have been investigated, as shown in Figs. 3(b)–3(e). Convergence tests show that 10 Å of vacuum, $8\times8\times1$ k points, and a cut-off energy of 400 eV ensure total-energy convergence to less than 1 meV/atom. With these parameters, we first calculated surface energies of Si-terminated SiC with increasing slab thickness using Eq. (2) and found that surface energy converges rapidly to 1.35 J/m^2 for a nine-layer slab. Next, we examined relaxations of SiC surface slabs with varying thickness by calculating the interlayer spacing. SiC(0001) surfaces show a low degree of interlayer relaxation with a maximum of 3% of bulk spacing for slabs containing nine or more layers.

2. Ti_3SiC_2(0001)

The Ti_3SiC_2(0001) surface can be terminated with C, Si, any of two types of Ti (Ti1 and Ti2), or their combinations, yielding a total of six possible surface geometries, as illustrated in Figs. 4(b)–4(g). The surface energy of Ti1(C) termination calculated using Eq. (3) is found to converge well to 0.84 J/m^2 by a 13-layer-thick slab. Further, interlayer relaxations also show good convergence for slabs having 13 layers or more, in agreement with another first-principles study.[66] Lastly, we also calculated the surface energies of the remaining terminations in Figs. 4(c)–4(g) to be 4.10, 0.64, 1.12, 1.56, and 5.60 J/m^2, respectively, in good agreement with reported results.[66] In summary, we have calculated the bulk and surface properties of SiC and Ti_3SiC_2 and shown that these values are consistent with existing experimental and theoretical data, thereby verifying the applicability of the method and model to further investigation.

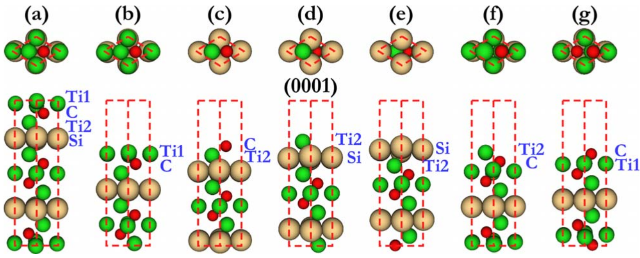

FIG. 4. (Color online) Top (upper) and side (bottom) view of Ti_3SiC_2: (a) bulk, (b) Ti1(C), (c) C(Ti2), (d) Ti2(Si), (e) Si(Ti2), (f) Ti2(C), and (g) C(Ti1) terminations. The letter in bracket denotes the subsurface atom. Only the top nine layers of each symmetric slab are presented for each termination.

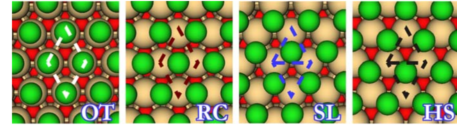

FIG. 5. (Color online) Schematic plots of four stacking sequences. Only the Ti layer of Ti_3SiC_2 proximal to interface is presented for clarity. The dotted parallelogram outlines the SiC rhombic unit cell projected along the [0001] direction.

IV. INTERFACE CONSTRUCTION AND CALCULATION PROCESS

As mentioned above, the orientation relationships between SiC and Ti_3SiC_2 were observed to be $(0001)_{Ti_3SiC_2} \| (0001)_{SiC}$ and $[0\bar{1}10]_{Ti_3SiC_2} \| [0\bar{1}10]_{SiC}$ by selected area electron diffraction.[22] Since detailed data on neither the chemical composition of SiC or Ti_3SiC_2 termination nor their interfacial stacking sequence are available, we have constructed a total of 96 possible candidate models, including four SiC terminations, six Ti_3SiC_2 terminations, and four stacking sequences. In the four stacking sequences, interfacial Ti (C or Si) of Ti_3SiC_2 are located (i) on top (OT) of the surface atoms of SiC, (ii) at the center of the rhombic (RC) unit cell, (iii) above second-layer (SL) atoms of SiC, and (iv) above hollow sites (HS) of SiC, as shown in Fig. 5. These stacking sequences are of high symmetry and thus more likely to correspond to total-energy extrema. According to surface calculations, our interface models consist of a nine-layer SiC(0001) slab connected to a Ti_3SiC_2(0001) slab of at least 13 layers. A 10 Å area of vacuum was added so as to minimize the coupling perpendicular to the interface. Along the interface plane, the slabs utilize 1×1 cells, which are composed of a finite number of layers of infinite extent. To form coherent interfaces, in-plane lattice constants of Ti_3SiC_2 are expanded by 0.63% to match those of the harder SiC. Because of the small lattice-constant mismatch, we neglect the full effect of misfit dislocation as a first approximation. Further, we performed calculations on the SiC/Ti_3SiC_2 interfaces using 2×2 slabs and found that the interfacial atoms have identical locations as we determined using the 1×1 slabs. Namely, we saw no clear evidence of reconstruction in the enlarged interface models. To better describe all interfaces, we shall divide our 96 models into two groups based on SiC terminations: Si- and C-terminated interfaces.

We took two steps to estimate the adhesion energy ($\mathbf{W}_{ad}$) defined in Eq. (1). First, total energies were calculated for various separations as two rigid slabs were brought increasingly closer from a large initial separation. The total energy was found to behave like a parabola, passing through a minimum at the equilibrium separation. The *unrelaxed* $\mathbf{W}_{ad}$ was obtained by computing the energy difference between the interface at equilibrium separation and unrelaxed isolated slabs. Next, full relaxation of each isolated slab and interface slab was allowed, which yielded an estimate for *relaxed* $\mathbf{W}_{ad}$. For the purpose of comparison, all total energies were calculated using the same cut-off energy (400 eV), $8\times8\times1$ k points, 10 Å area of vacuum, and—where possible—the same slab size. Convergence tests found that these parameters were sufficient to converge the total energy well to less than 1 meV/atom and thus applied to all ensuing calculations.

V. SILICON-TERMINATED INTERFACES

A. Adhesion energies

Table I lists the adhesion energies of Si-terminated interfaces before and after relaxation. A general trend observed in this table is that C-terminated Ti_3SiC_2 exhibits the strongest adhesion followed by Ti- and Si-terminated Ti_3SiC_2 as second and third, respectively, independent of whether SiC is terminated with Si1 or Si2. Of all the interfaces, the one that consists of Si1-terminated SiC and C(Ti1)-terminated Ti_3SiC_2 [Si1-C(Ti1)] has the largest relaxed $\mathbf{W}_{ad}$ of 4.99 J/m^2 and its ordering of stacking sequence has been altered by relaxation. Instead of the HS site with the strongest adhesion, the RC site—which is predicted to be the third before relaxation—is now preferred, suggesting that there might be a substantial change in structure. Since neither experimental nor theoretical $\mathbf{W}_{ad}$ values are available for this interface, it is hard to confirm the accuracy of our calculated results directly. However, we have noticed that our relaxed $\mathbf{W}_{ad}$ of the Si1-Ti2(Si) case (2.44 J/m^2) agrees well with the $\mathbf{W}_{ad}$ value of 2.52 J/m^2 calculated from the SiC/Ti interface.[33] Moreover, the $\mathbf{W}_{ad}$ value of the Si1-Si(Ti2) case (1.01 J/m^2), though relatively smaller, is comparable to the result for the SiC/Si interface (1.55 J/m^2) obtained using *ab initio* methods.[25]

Since the k point and cut-off energy are sufficient to ensure a total-energy precision of higher than 1 meV/atom, another potential inaccuracy may arise from the size effect of the slabs used. To assess this effect, we quadrupled the original 1×1 slabs along the interface plane to 2×2 slabs and recalculated the $\mathbf{W}_{ad}$ of Si1-terminated interfaces. We found that the calculated unrelaxed $\mathbf{W}_{ad}$ for C(Ti1) at the RC site, Ti2(Si) at RC, and Si(Ti2) at OT using 2×2 (1×1) slabs were 3.54 (3.54), 2.25 (2.25), and 1.03 (1.04) J/m^2, and their corresponding relaxed values were 5.00 (4.99), 2.54 (2.44), and 1.01 (1.01) J/m^2, respectively. The largest difference in $\mathbf{W}_{ad}$ caused by the size effect was 0.1 J/m^2; only 4.1% larger than its original value. Further, we examined the influence of slab size on $\mathbf{W}_{ad}$ rank ordering of the four stacking sequences and found that a fourfold-enlarged slab kept

TABLE I. Unrelaxed and relaxed values of adhesion energy, $\mathbf{W}_{ad}$ (in J/m^2), as defined in Eq. (1), for the interfaces between Si-terminated SiC(0001) and Ti_3SiC_2(0001) terminated with any of six possibilities: Ti1(C), Ti2(Si), Ti2(C), Si(Ti2), C(Ti2), and C(Ti1).

Termination		Unrelaxed				Relaxed			
SiC	Ti_3SiC_2	OT	RC	SL	HS	OT	RC	SL	HS
	Ti1(C)	1.10	2.17	2.42	2.27	1.07	2.31	2.33	2.17
	Ti2(Si)	1.06	2.25	2.36	2.47	1.02	2.44	2.33	2.43
Si1	Ti2(C)	1.14	2.17	2.23	2.45	1.09	2.34	2.13	2.35
	Si(Ti2)	1.04	0.85	1.00	0.89	1.01	0.97	0.98	0.85
	C(Ti2)	2.08	2.86	2.95	3.97	1.81	3.87	3.42	3.86
	C(Ti1)	2.12	3.54	3.74	4.63	2.18	4.99	4.65	4.97
	Ti1(C)	1.58	2.25	2.85	2.04	1.52	2.71	2.75	1.98
	Ti2(Si)	1.59	2.26	2.95	2.04	1.52	2.86	2.90	2.02
Si2	Ti2(C)	2.04	2.22	2.77	2.04	1.96	2.62	2.65	1.96
	Si(Ti2)	2.63	1.61	1.36	1.66	2.58	1.64	1.33	1.62
	C(Ti2)	3.66	3.00	2.11	3.14	3.45	2.83	1.95	2.82
	C(Ti1)	3.63	3.08	2.23	3.09	3.65	3.14	2.28	3.08

the same ordering as that we determined from the 1×1 model.

B. Local atomic structure

For the interface having the strongest adhesion, our fully optimized structure is shown in Fig. 6, where one can see that the geometry of interfacial C of Ti_3SiC_2 is altered substantially as a result of relaxation. The interfacial C atoms are strongly pulled away from the RC site toward the SiC surface, shifting the interface location somewhat closer to SiC (dotted lines). The heavily displaced C atoms ultimately fill the positions that would normally be occupied by C in bulk SiC, presumably to satisfy dangling bonds on interfacial Si. The interfacial C-Si distance and bond angle of tetragonally coordinated C-Si-C are calculated to be 1.90 Å and 109.8°, strikingly close to the values 1.89 Å and 109.54° obtained from bulk 4H-SiC.[57,67] The subinterfacial C-Ti bonds, however, deviate in length by 0.26 Å from their bulk Ti_3SiC_2 value of 2.18 Å.[65] This deviation is screened rapidly to less than 0.03 Å within the next layer, meaning that the effect of the interface is localized. Despite the length deviation, the stacking sequence of Ti_3SiC_2 around the interface is identical to that of its bulk. This, together with the occupation of C in the anion site of bulk SiC, implies that the interfacial C layer plays a crucial role in the smooth transition from SiC to Ti_3SiC_2. We also found that the rumpling of interfacial layers is relatively small (<0.01 Å), which is consistent with the atomically flat interface observed by HRTEM.[22]

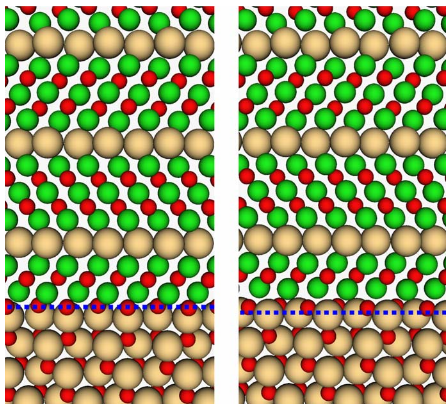

FIG. 6. (Color online) Left: unrelaxed interface between Si1-terminated SiC and C(Ti1)-terminated Ti_3SiC_2. Interfacial C atoms of Ti_3SiC_2 occupy RC site of SiC. Right: corresponding relaxed geometry. The direction of view is along $[11\bar{2}0]$ and location of interface is marked with dotted lines. Top and bottom parts have been omitted.

C. Electronic properties

1. Charge-density difference

To investigate the degree to which changes in structural characteristics are localized and to analyze the mixture of electronic states at the interface, we have calculated the charge-density difference by subtracting the sum of the charge density of isolated SiC and Ti_3SiC_2 slabs from the total interface charge density. Figure 7 shows the results of plane-averaged density difference along the normal to the interface. The location of the respective atom is shown as well for easy reference, and the interface position is set to zero. A comparison of Figs. 7(a) and 7(b) confirms that interfacial C is displaced toward SiC in the Si1-C(Ti1) interface after relaxation, forming an interfacial Si-C pair similar to the pair in the SiC bulk. As a consequence of this shift of interfacial C and corresponding charge transfer, there appears a dramatic depletion of charge in the region between interfacial C and Ti [denoted by a arrow in Fig. 7(b)], which indicates that the covalent element of the C-Ti bonds is weakened. Meanwhile, charge is also found to be depleted significantly in the region between interfacial Si and sub-

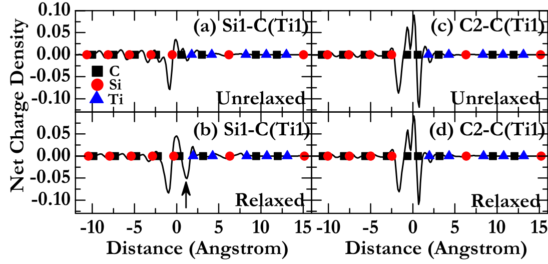

FIG. 7. (Color online) Variation in charge density as a function of distance from interface along [0001] direction for (a) unrelaxed Si1-C(Ti1), (b) relaxed Si1-C(Ti1), (c) unrelaxed C2-C(Ti1), and (d) relaxed C2-C(Ti1) interfaces. The interfacial C atoms of Ti_3SiC_2 initially occupy the RC site of the outmost layer of SiC for the Si1-terminated interface but the OT site for the C2-terminated interface. The interface location is set to zero.

interfacial C on the SiC side. The depleted charges accumulate at the interface, suggesting strengthened Si-C bonding. These charge variations due to interface formation decay rapidly with distance from the interface, and the entire interfacial region is basically neutral.

2. Partial density of states

To gain further insight into the electronic states, we present in Fig. 8 the DOS projected on selected atomic layers of the Si1-C(Ti1) interface. A key feature of this figure is that the PDOS of the interfacial C layer of Ti_3SiC_2 is very similar to that of a C layer deeper in SiC but far from that of a C layer deeper in Ti_3SiC_2, which suggests the strong influence of the SiC substrate on the interfacial electronic states. This pronounced effect even emerges before relaxation (see lower part of Fig. 8) when the interfacial C atoms still sit at the RC site. In addition to this feature, significant hybridization can

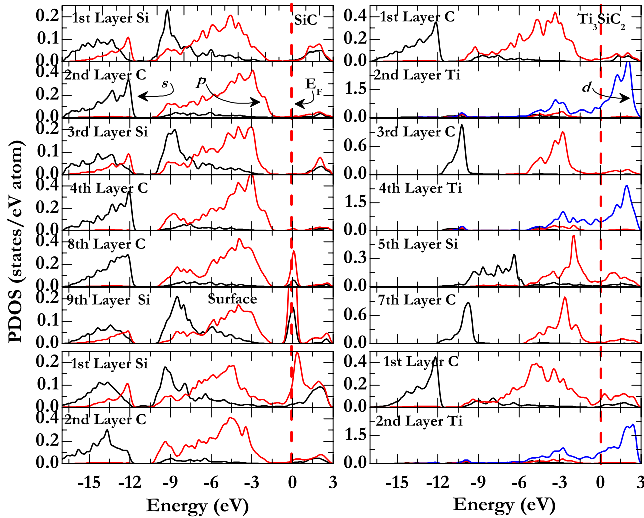

FIG. 8. (Color online) DOS projected on atomic layers of the Si1-C(Ti1) interface before (lower two panels) and after (upper six panels) relaxation. The left panel shows PDOS of SiC layers, while the right panel shows that of Ti_3SiC_2 layers. The first layer is the atomic layer closest to the interface. The Fermi level is set to zero and represented by vertical lines.

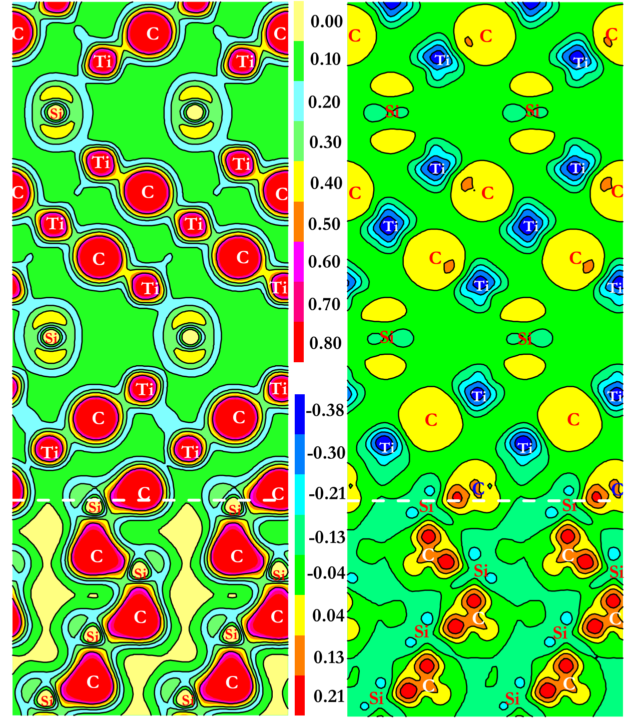

FIG. 9. (Color online) Contour plot of charge density (left) and its difference (right) along the $(11\bar{2}0)$ plane of the Si1-C(Ti1) interface. The difference of charge density shows redistribution of charge in the interface relative to the isolated system. The interface is indicated by a horizontal line and the atoms that intersect the contour plane are labeled. The upper scale denotes the magnitude of charge in the left panel, while the lower scale denotes that in the right panel.

be observed between interfacial Si *sp* and C *sp* states, suggesting covalent bonding at the interface. It is worth noting that there is a small degree of overlap between interfacial C *p* and Ti *d* states inside the Ti_3SiC_2 slab, which persists as the distance from the interface increases. This overlap induces weak gap states at E_F, meaning that the C layers inside Ti_3SiC_2 are somewhat metallized. The slight metallization of C is also present in bulk Ti_3SiC_2 (see Fig. 2) but is completely absent in both the SiC slab and bulk. However, there is a sharp peak in the energy gap of SiC surface layers (eighth and ninth layers), which is due to the surface states of dangling bonds, as observed in the Si-terminated 6H-SiC(0001) surface.[68] Apart from the presence of metal-induced gap states (MIGSs) in the C layers, the Si layers of Ti_3SiC_2 exhibit similar MIGSs at E_F, which is ascribed to the overlap between Ti *d* and Si *p* states.

3. Charge distribution

Though the PDOS can reveal detailed information on how covalent bonds form, it offers restricted insight into matters regarding ionicity and charge distribution. To identify bonding type directly, we present in Fig. 9 a contour plot of charge density and its difference along the $(11\bar{2}0)$ plane for the Si1-C(Ti1) interface. The $(11\bar{2}0)$ plane has been selected deliberately because it slices through interfacial atoms, Si-C

TABLE II. Unrelaxed and relaxed values of adhesion energy, $\mathbf{W}_{ad}$ (in J/m^2), as defined in Eq. (1), for the interfaces between C-terminated SiC(0001) and Ti_3SiC_2(0001). The nomenclature is identical to that in Table I.

Termination		Unrelaxed				Relaxed			
SiC	Ti_3SiC_2	OT	RC	SL	HS	OT	RC	SL	HS
	Ti1(C)	2.82	3.11	3.69	3.10	2.46	3.29	3.30	2.75
	Ti2(Si)	2.88	3.13	3.82	3.28	2.52	3.45	3.46	3.07
C1	Ti2(C)	2.84	3.12	3.38	3.17	2.48	2.75	2.95	2.86
	Si(Ti2)	3.39	1.72	1.73	1.06	3.04	2.84	1.36	0.72
	C(Ti2)	3.73	1.68	1.50	0.60	3.00	2.98	1.62	0.36
	C(Ti1)	4.06	1.92	1.38	0.71	3.76	3.68	1.44	0.51
	Ti1(C)	3.76	5.05	5.06	5.08	3.65	5.08	5.22	5.16
	Ti2(Si)	3.78	5.93	6.36	6.29	3.71	5.92	6.34	6.30
C2	Ti2(C)	3.79	4.79	4.97	4.69	3.70	4.81	4.88	4.74
	Si(Ti2)	4.18	5.19	5.89	6.69	3.66	6.81	6.08	6.66
	C(Ti2)	6.50	5.60	5.14	5.27	6.10	5.92	5.89	5.32
	C(Ti1)	7.24	6.03	5.49	5.91	7.14	6.68	6.60	6.36

pairs deeper in the SiC, and many Ti_3SiC_2 atoms, thereby allowing us to extract maximum bonding information on this interface. As can be seen in Fig. 9, there is a significant difference in charge distribution between SiC and Ti_3SiC_2, especially for the C atom. The charge distribution around the C of Ti_3SiC_2 is almost spherically symmetric, while that surrounding the C of SiC has humps directed toward neighboring Si. Evidently, the two distinct classes of charge distribution on C atoms are responsible for their different DOS.

Interfacial Si-C bonds exhibit a character practically identical to that of Si-C bonds deeper in SiC: (i) most of the charges are localized on C atoms and (ii) charges on C are distorted toward neighboring Si. These two observations suggest that the interfacial bonds are of a mixed covalent-ionic nature. We also find a significant amount of charge accumulated along the interfacial Si-C bond, as in the case of the Si-C pairs visible in bulk SiC (right panel of Fig. 9). This similarity corroborates our previous findings from the DOS analyses showing that interfacial C has an electronic structure approaching that of C in bulk SiC. The charge accumulated along the interfacial Si-C bond strengthens the interfacial adhesion, which is consistent with the large $\mathbf{W}_{ad}$ associated with this interface. Finally, we note that a small degree of covalency is present in the Ti of Ti_3SiC_2, which is due to hybridization of Ti d states with C (Si) p states, as shown in Fig. 8. The charge distribution between Ti and C is larger than that between Ti and Si, indicating that Ti-C is a stronger chemical bond than Ti-Si.

VI. CARBON-TERMINATED INTERFACES

A. Adhesion energies

Results of $\mathbf{W}_{ad}$ on C-terminated interfaces before and after structure relaxation are shown in Table II. As in the case of the Si-terminated interfaces, the C-terminated Ti_3SiC_2 also shows the strongest adhesion to SiC. The difference is that the preference ordering of the Ti- and Si-terminated Ti_3SiC_2 depends on the SiC termination; that is, the Ti-terminated Ti_3SiC_2 ranks the second when SiC is terminated with C1, but the third when terminated with C2. In addition, unlike the substantial difference in $\mathbf{W}_{ad}$ between the three classes of Ti_3SiC_2 terminations in Si-terminated interfaces, the differences here are minor. Moreover, the ordering of the most preferred stacking sequence has also been altered, with the OT site exhibiting strongest adhesion for C-terminated cases and the SL site for Ti-terminated cases. The largest $\mathbf{W}_{ad}$ of all the C-terminated interfaces belongs to the C2-C(Ti1) interface: 7.14 J/m^2. Finally, through quadrupling the original slabs along the interface plane and recalculating the $\mathbf{W}_{ad}$ of C1-terminated interfaces, we found that the unrelaxed $\mathbf{W}_{ad}$ for C(Ti1) at OT site, Ti2(Si) at SL, and Si(Ti2) at OT using 2×2 (1×1) slabs are 4.06 (4.06), 3.81 (3.82), and 3.38 (3.39) J/m^2, and the corresponding relaxed values are 3.76 (3.76), 3.46 (3.46), and 3.04 (3.04) J/m^2, respectively, which validates the use of original slabs to predict $\mathbf{W}_{ad}$.

B. Local atomic structure

The unrelaxed and fully relaxed geometries of the C2-C(Ti1) interface are shown in Fig. 10. Unlike the Si1-C(Ti1) interface in which there is significant change in interfacial configuration due to optimization, the atomic rearrangement here is negligible, and the slabs retain the stacking sequence of the bulk. The interfacial C atoms of Ti_3SiC_2 sit 1.25 Å straight above the interfacial C of SiC in a triple-bonded-dimer fashion and have a bond length of 2.23 Å with neighboring Ti, which is somewhat longer than the bulk distance of 2.18 Å.[65] The interfacial C-C bond length changes by less than 0.001 Å during relaxation. The interfacial C atoms of SiC are also located directly above the neighboring Si with a distance of 1.84 Å; only 0.05 Å shorter than the value observed in the 4H-SiC bulk.[58] Moreover, the atoms second nearest to the interface on either side maintain nearly the same bond lengths and angles as those in the bulk, indicating

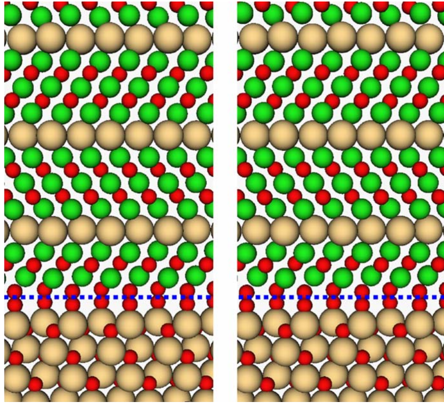

FIG. 10. (Color online) Left: unrelaxed atomic geometry of the C2-C(Ti1) interface. The interfacial C atoms of Ti_3SiC_2 occupy the OT site of surface atoms of SiC. Right: corresponding relaxed structure.

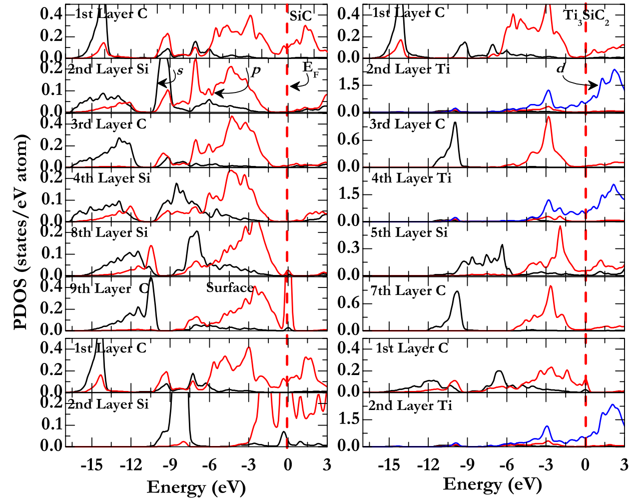

FIG. 11. (Color online) The DOS projected on atomic layers of C2-C(Ti1) interface before (lower two panels) and after (upper six panels) relaxation. The left panel shows the PDOSs of SiC layers, while the right panel shows those of Ti_3SiC_2 layers. The first layer is the atomic layer proximal to the interface. The Fermi level is set to zero and represented by vertical dashed lines.

that the influence of the interface is localized to within interfacial layers.

C. Electronic properties

1. Charge-density difference

The plane-averaged density difference for the C2-C(Ti1) interface is presented in Figs. 7(c) and 7(d). Unlike the Si1-C(Ti1) interface, structure relaxation here does not result in a noticeable change in charge, which can be inferred from the negligible rearrangement of atomic structure. Upon comparing the two interfaces, we also find that the density difference in the C2-C(Ti1) interface deviates more prominently from zero around the interface, reflecting a more pronounced charge transfer between the SiC and Ti_3SiC_2 slabs. One common feature is the large degree of charge accumulation at the interface at the expense of depletion of charge in the subinterfacial layers. This suggests that the atoms second nearest to interface have a significant contribution to the interfacial bonding.

2. Partial density of states

The layer-projected DOS (Fig. 11) for the C2-C(Ti1) interface shares some features with that of the Si1-C(Ti1) system: (i) effect of interface on electronic states of both SiC and Ti_3SiC_2 are localized to within the second layer, (ii) there are some dangling-bond surface states in the energy gap of SiC, and (iii) the C and Si atoms of Ti_3SiC_2 are slightly metallized because of the overlap of Ti d with C (Si) p states. The main difference is that the overall PDOS feature of the interfacial C layer of Ti_3SiC_2 does not resemble the C layer in bulk SiC or Ti_3SiC_2. Moreover, a slight bump at E_F can be seen in the PDOS of interfacial C of Ti_3SiC_2, which may be attributed to the interaction between Ti d and C p states. This interaction continues into the SiC, inducing a peak around E_F in the PDOS of interfacial C of SiC and also leading to a complicated PDOS for subinterfacial Si of SiC. The peak at E_F is due to the metallization of the interfacial C layer of SiC, which nearly vanishes in the layers away from interface. At the interface, there is a large degree of overlap between the two C p states just below E_F. When comparing the PDOS before and after relaxation, we find that electronic structures are altered significantly by optimization even though the change in atomic structure is negligible.

3. Charge distribution

Figure 12 shows contour plots of charge density and its difference for the C2-C(Ti1) interface intersected along the same plane as in Fig. 9. As in the case of the Si1-C(Ti1) interface, most of the charge is still concentrated on the C atoms in two distinct manners: the charge region on the C of Ti_3SiC_2 is of predominantly spherical symmetry, while that on the C of SiC exhibits pronounced lobes directed toward neighboring Si. At the interface, we observe a large charge accumulation along the interfacial C-C bond lines, which is consistent with the positive peak in Fig. 7(d). As seen in right panel of Fig. 12, this charge accumulation is so dramatic that it even exceeds that on the Si-C bonds of the SiC slab, which is apparently responsible for the strong adhesion in the C2-C(Ti1) interface. This, together with the charge localization on interfacial C, indicates that the interface exhibits a mixture of covalent and ionic-type bondings. However, we find that the consolidated interfacial bonding occurs partly at the expense of depletion of charge between the interfacial C and the remainder of the Ti_3SiC_2 slab, thereby weakening the subinterfacial C-Ti bonding, as seen in Fig. 7(d).

VII. CONCLUSIONS

We have conducted a first-principles study of the 4H-SiC(0001)/Ti_3SiC_2(0001) interface aimed at determining the stable interface configuration, evaluating the adhesion energetics, and providing insight into the nature of interfacial

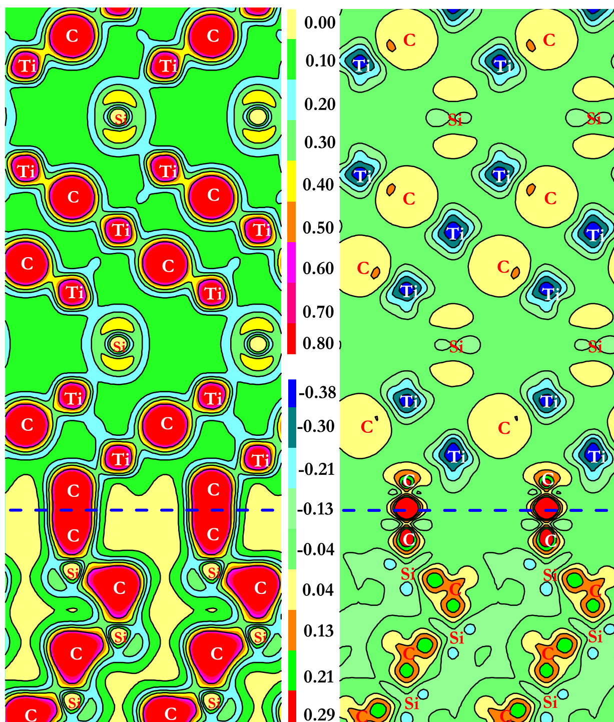

FIG. 12. (Color online) Contour plots of charge density (left) and difference of charge density (right) for the C2-C(Ti1) interface taken along the $(11\bar{2}0)$ plane.

bonding. After validating application of the methodology and models by conducting calculations on bulk and surface properties, we established a total of 96 candidate interfacial geometries using bulklike slabs, taking into account the termination effect, stacking sequence, and full optimization. We found that independent of the SiC terminations, C-terminated Ti_3SiC_2 has the largest $\mathbf{W}_{ad}$, indicating the fundamental effect of C on strong adhesion in this interface system. For the optimal Si1-C(Ti1) interface, the interfacial C atoms of Ti_3SiC_2 are pulled toward the SiC surface and ultimately occupy the sites where there would normally be C in bulk SiC, shifting the interface toward the substrate. Simultaneously, the interfacial C maintains a stacking sequence identical to that in the Ti_3SiC_2 bulk, thereby playing an essential role in realizing a smooth transition from SiC to Ti_3SiC_2. For the optimal C2-C(Ti1) interface, however, no significant atomic displacement due to relaxation is observed around the interface; in which the interfacial C of Ti_3SiC_2 rests straight above the interfacial C of SiC.

Several analytic methods were used to characterize the nature of the interfacial bonding. We found that the interfacial bonds were primarily of a mixed covalent-ionic type. The covalency of the interfacial bonds in the Si1-C(Ti1) interface stemmed mainly from the hybridization between Si *sp* and C *sp* states. The PDOS of the interfacial C of Ti_3SiC_2 resembled that of C in bulk SiC rather than bulk Ti_3SiC_2 and interfacial Si-C bonding was similar to what is seen in bulk SiC. This, together with the similarity of the atomic structure to that in bulk SiC, suggests that the interfacial C of Ti_3SiC_2 can be regarded as a continuation of SiC. However, the PDOS of the interfacial C of Ti_3SiC_2 in the C2-C(Ti1) interface does not resemble that of C in bulk SiC or bulk Ti_3SiC_2. Furthermore, a large charge is found to accumulate on the interfacial C-C bonds, strengthening adhesion in the C2-C(Ti1) interface.

ACKNOWLEDGMENTS

We thank S. Watanabe (University of Tokyo) for allowing our use of the VASP code and computational resources. The present study was supported in part by a Grant-in-Aid for Scientific Research on Priority Area, "Atomic Scale Modification (474)" from the Ministry of Education, Culture, Sports, Science, and Technology of Japan. The calculations were carried out on a parallel SR11000 supercomputer at the Institute for Solid State Physics, University of Tokyo.

*zcwang@wpi-aimr.tohoku.ac.jp
†ikuhara@sigma.t.u-tokyo.ac.jp

[1] H. G. Bohn, J. M. Williams, C. J. McHargue, and G. M. Begun, J. Mater. Res. **2**, 107 (1987).
[2] K. Shenai, R. S. Scott, and B. J. Baliga, IEEE Trans. Electron Devices **36**, 1811 (1989).
[3] T. P. Chow, V. Khemka, J. Fedison, N. Ramungal, K. Matocha, Y. Tang, and R. J. Gutmann, Solid-State Electron. **44**, 277 (2000).
[4] H. Morkoc, S. Strite, G. B. Gao, M. E. Lin, B. Sverdlov, and M. Burns, J. Appl. Phys. **76**, 1363 (1994).
[5] P. G. Neudeck, J. Electron. Mater. **24**, 283 (1995).
[6] M. Ruff, H. Mitlehner, and R. Helbig, IEEE Trans. Electron Devices **41**, 1040 (1994).
[7] C. E. Weitzel, IEEE Electron Device Lett. **16**, 451 (1995).
[8] H. Hochst, D. W. Niles, G. W. Zajac, T. H. Fleisch, B. C. Johnson, and J. M. Meese, J. Vac. Sci. Technol. B **6**, 1320 (1988).
[9] C. E. Weitzel, J. W. Palmeur, C. Carter, K. Mooce, K. J. Mordquist, and S. Allen, IEEE Trans. Electron Devices **43**, 1732 (1996).
[10] Y. Singh and M. J. Kumar, IEEE Trans. Electron Devices **48**, 2695 (2001).
[11] R. Singh, J. A. Cooper, M. R. Melloch, T. P. Chow, and J. W. Palmour, IEEE Trans. Electron Devices **49**, 665 (2002).
[12] D. T. Morisette and J. A. Cooper, IEEE Trans. Electron Devices **49**, 1657 (2002).
[13] V. Khemka, V. Ananthan, and T. P. Chow, IEEE Electron Device Lett. **21**, 286 (2000).
[14] H. Yu, J. Lai, X. Li, Y. Luo, L. Fursin, and J. H. Zhao, Conf. Rec. Ind. Appl. Soc. IEEE IAS Annu. Meet. **4**, 2609 (2002).
[15] L. M. Porter and R. F. Davis, Mater. Sci. Eng., B **34**, 83 (1995).
[16] J. Crofton, L. M. Porter, and J. R. Williams, Phys. Status Solidi B **202**, 581 (1997).
[17] O. Nakatsuka, T. Takei, Y. Koide, and M. Murakami, Mater. Trans. **43**, 1684 (2002).

[18] K. Vassilevski, K. Zekentes, K. Tsagaraki, G. Constantinidis, and I. Nikitina, Mater. Sci. Eng., B **80**, 370 (2001).
[19] R. Konishi, R. Yasukochi, O. Nakatsuka, Y. Koide, M. Moriyama, and M. Murakami, Mater. Sci. Eng., B **98**, 286 (2003).
[20] M. R. Jennings, A. Perez-Tomas, M. Davies, D. Walker, L. Zhu, P. Losee, W. Huang, S. Balachandran, O. J. Guy, J. A. Covington, T. P. Chow, and P. A. Mawby, Solid-State Electron. **51**, 797 (2007).
[21] S. E. Mohney, B. A. Hull, J. Y. Lin, and J. Crofton, Solid-State Electron. **46**, 689 (2002).
[22] S. Tsukimoto, K. Nitta, T. Sakai, M. Moriyama, and M. Murakami, J. Electron. Mater. **33**, 460 (2004).
[23] B. J. Johnson and M. A. Capano, J. Appl. Phys. **95**, 5616 (2004).
[24] F. F. Zhao, Y. P. Feng, Y. F. Dong, and J. Z. Zheng, Phys. Rev. B **74**, 033301 (2006).
[25] L. Pizzagalli, G. Cicero, and A. Catellani, Phys. Rev. B **68**, 195302 (2003).
[26] M. W. Finnis, J. Phys.: Condens. Matter **8**, 5811 (1996).
[27] T. Hong, J. R. Smith, and D. J. Srolovitz, Acta Metall. Mater. **43**, 2721 (1995).
[28] W. Liu, J. C. Li, W. T. Zheng, and Q. Jiang, Phys. Rev. B **73**, 205421 (2006).
[29] K. Nagao, J. B. Neaton, and N. W. Ashcroft, Phys. Rev. B **68**, 125403 (2003).
[30] G. Profeta, A. Continenza, and A. J. Freeman, Phys. Rev. B **64**, 045303 (2001).
[31] Lu Wenchang, Zhang Kaiming, and Xie Xide, Phys. Rev. B **45**, 11048 (1992).
[32] J. Hoekstra and M. Kohyama, Phys. Rev. B **57**, 2334 (1998).
[33] M. Kohyama and J. Hoekstra, Phys. Rev. B **61**, 2672 (2000).
[34] S. Tsukimoto, T. Sakai, and M. Murakami, J. Appl. Phys. **96**, 4976 (2004).
[35] M. Gao, S. Tsukimoto, S. H. Goss, S. P. Tumakha, T. Onishi, M. Murakami, and L. J. Brillson, J. Electron. Mater. **36**, 277 (2007).
[36] G. Kresse and J. Furthmuller, Phys. Rev. B **54**, 11169 (1996).
[37] G. Kresse and J. Hafner, Phys. Rev. B **47**, 558 (1993).
[38] P. E. Blöchl, Phys. Rev. B **50**, 17953 (1994).
[39] J. P. Perdew, J. A. Chevary, S. H. Vosko, K. A. Jackson, M. R. Pederson, D. J. Singh, and C. Fiolhais, Phys. Rev. B **46**, 6671 (1992).
[40] H. J. Monkhorst and J. D. Pack, Phys. Rev. B **13**, 5188 (1976).
[41] M. Methfessel and A. T. Paxton, Phys. Rev. B **40**, 3616 (1989).
[42] P. Pulay, Chem. Phys. Lett. **73**, 393 (1980).
[43] D. Singh, Phys. Rev. B **40**, 5428 (1989).
[44] O. Jepson and O. K. Andersen, Solid State Commun. **9**, 1763 (1971).
[45] P. E. Blöchl, O. Jepsen, and O. K. Andersen, Phys. Rev. B **49**, 16223 (1994).
[46] M. C. Payne, M. P. Teter, D. C. Allan, T. A. Arias, and J. D. Joannopoulos, Rev. Mod. Phys. **64**, 1045 (1992).
[47] R. P. Feynman, Phys. Rev. **56**, 340 (1939).
[48] L. S. Ramsdell, Am. Mineral. **32**, 64 (1947).
[49] N. W. Jepps and T. F. Page, Prog. Cryst. Growth Charact. **7**, 259 (1983).
[50] R. W. G. Wyckoff, *Crystal Structures*, 2nd ed. (Interscience, New York, 1963), Vol. 1, p. 113.
[51] A. Bauer, J. Kraublich, L. Dressler, P. Kuschnerus, J. Wolf, and K. Goetz, Phys. Rev. B **57**, 2647 (1998).
[52] M. Y. Gamarnik and M. W. Barsoum, J. Mater. Sci. **34**, 169 (1999).
[53] T. Goto and T. Hirai, Mater. Res. Bull. **22**, 1195 (1987).
[54] R. Ahuja, O. Eriksson, J. M. Wills, and B. Johansson, Appl. Phys. Lett. **76**, 2226 (2000).
[55] B. E. Wheeler, Solid State Commun. **4**, 173 (1966).
[56] B. Baumeier, P. Krüger, and J. Pollmann, Phys. Rev. B **73**, 195205 (2006).
[57] P. Käckell, B. Wenzien, and F. Bechstedt, Phys. Rev. B **50**, 10761 (1994).
[58] W. Y. Ching, Y. N. Xu, P. Rulis, and L. Z. Ouyang, Mater. Sci. Eng., A **422**, 147 (2006).
[59] M. S. Hybertsen and S. G. Louie, Phys. Rev. B **34**, 5390 (1986).
[60] F. Bechstedt and R. Del-Sole, Phys. Rev. B **38**, 7710 (1988).
[61] I. Shalish, I. B. Altfeder, and V. Narayanamurti, Phys. Rev. B **65**, 073104 (2002).
[62] B. Kaczer, H. J. Im, J. P. Pelz, J. Chen, and W. J. Choyke, Phys. Rev. B **57**, 4027 (1998).
[63] M. W. Barsoum and T. El-Raghy, J. Am. Ceram. Soc. **79**, 1953 (1996).
[64] Y. C. Zhou and Z. M. Sun, J. Phys.: Condens. Matter **12**, L457 (2000).
[65] N. I. Medvedeva, D. L. Novikov, and A. J. Freeman, Phys. Rev. B **58**, 16042 (1998).
[66] H. Z. Zhang and S. Q. Wang, Acta Mater. **55**, 4645 (2007).
[67] C. M. Tanner, J. Choi, and J. P. Chang, J. Appl. Phys. **101**, 034108 (2007).
[68] Y. Li, L. Ye, and X. Wang, Surf. Sci. **600**, 298 (2006).